Tunable high-channel-count bandpass plasmonic filters based on an analogue of electromagnetically induced transparency



2012 Nanotechnology 23 444003

(http://iopscience.iop.org/0957-4484/23/44/444003)

Nanotechnology **23** (2012) 444003 (6pp) doi:10.1088/0957-4484/23/44/444003

# Tunable high-channel-count bandpass plasmonic filters based on an analogue of electromagnetically induced transparency

**Hua Lu, Xueming Liu, Guoxi Wang and Dong Mao**

State Key Laboratory of Transient Optics and Photonics, Xi'an Institute of Optics and Precision Mechanics, Chinese Academy of Sciences, Xi'an 710119, People's Republic of China

E-mail: liuxueming72@yahoo.com and liuxm@opt.ac.cn

Received 17 January 2012, in final form 18 February 2012
Published 18 October 2012
Online at stacks.iop.org/Nano/23/444003

**Abstract**

We have proposed a novel type of bandpass plasmonic filter consisting of metal–insulator–metal bus waveguides coupled with a series of side-coupled cavities and stub waveguides. The theoretical modeling demonstrates that our waveguide-resonator system performs a plasmonic analogue of electromagnetically induced transparency (EIT) in atomic systems, as is confirmed by numerical experiments. The plasmonic EIT-like response enables the realization of nanoscale bandpass filters with multiple channels. Additionally, the operating wavelengths and bandwidths of our filters can be efficiently tuned by adjusting the geometric parameters such as the lengths of stub waveguides and the coupling distances between the cavities and stub waveguides. The ultracompact configurations contribute to the achievement of wavelength division multiplexing systems for optical computing and communications in highly integrated optical circuits.

(Some figures may appear in colour only in the online journal)

## 1. Introduction

With the advances of nanotechnology, nanoplasmonics is emerging as a new research field focusing on light–matter interactions mediated by resonant excitations of surface plasmons (SPs) in metallic nanostructures [1]. SPs, electromagnetic waves coupled to the propagating free electron oscillations at metal–dielectric interfaces, have been considered as promising energy and information carriers to overcome the classical diffraction limit of light and control light at the nanoscale [2, 3]. Recently, SP-assisted nanoscale photonic elements such as the all-optical switching [4, 5], splitters [6], interferometers [3, 7], modulators [8], sensors [9], mirrors [10], amplifier [11], buffers [12] and Bragg reflectors [13, 14] have been investigated numerically and demonstrated experimentally. Among these configurations, metal–insulator–metal (MIM) waveguides are the most promising for the realization of truly nanoscale photonic devices due to their deep-subwavelength confinement of light and relatively simple fabrication [15, 16]. As one of the most important devices in communication, plasmonic filters based on MIM waveguides have been studied widely. Bragg gratings fabricated by alternatively stacking two kinds of dielectrics [13] and different gap widths [14] can realize filtering characteristics. To overcome the complexity of fabrication of Bragg reflectors and promote the miniaturization and integration of components, some simple plasmonic wavelength filtering structures based on resonator-coupled MIM waveguides have been proposed and investigated, such as tooth-shaped waveguide filters [17], plasmonic filters with disks [18], rectangular [19], and ring [20] resonators, as well as wavelength demultiplexers [21, 22]. There are two basic types of wavelength-selective elements in MIM plasmonic waveguides, i.e. bandpass and bandstop filters. The bandstop filters reflect special frequencies within a selected band, which is the typical property of Bragg reflectors [13, 14] and side-coupled resonators [17, 19]. The bandpass filters, which permit transmitting particular frequencies, are also important for nanoscale on-chip integrations [18, 20]. The above wavelength-selective plasmonic architectures

 

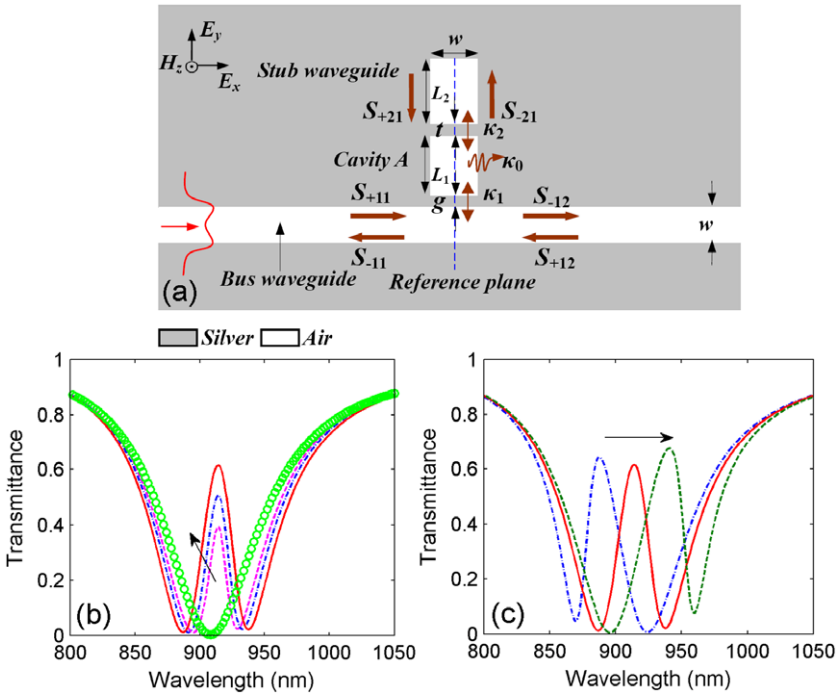


**Figure 1.** (a) Schematic diagram of the fundamental plasmonic configuration. (b) Spectral transmittance of the plasmonic waveguide-resonator system calculated by using the analytical theoretical modeling with $\kappa_2 = 0$ rad s$^{-1}$ (green and circled), $2 \times 10^{12}$ rad s$^{-1}$ (purple and dashed), $3 \times 10^{12}$ rad s$^{-1}$ (blue and dash–dotted), and $4.5 \times 10^{12}$ rad s$^{-1}$ (red and solid). The other parameters are $\omega_0 = 2.076 \times 10^{15}$ rad s$^{-1}$, $\kappa_0 = 5 \times 10^{12}$ rad s$^{-1}$, $\kappa_1 = 1 \times 10^{14}$ rad s$^{-1}$, $L_2 = 290$ nm, $w = 50$ nm, $\delta = 0.975$, and $\theta$=3.88 rad. (c) Spectral transmittance for $\kappa_2 = 4.5 \times 10^{12}$ rad s$^{-1}$, but with $L_2$ of 280 nm (blue and dash–dotted), 290 nm (red and solid), and 300 nm (green and dashed).

have one channel and thus only filter wavelengths in a single band. Multi-channel plasmonic filters have been proposed, such as dual-channel filters in a quasiperiodic metal heterowaveguide [23] and high-channel-count bandstop plasmonic filters with MIM Fibonacci-sequence gratings [24]. However, practical applications of the multi-channel plasmonic filters based on MIM Bragg gratings are restricted due to their large dimensions and geometrical complexity. Most importantly, there is currently not an effective scheme to realize high-channel-count bandpass plasmonic filters which are one of most important components in highly integrated optical communications and computing.

In this paper, we propose a novel and simple method for the design of nanoscale high-channel-count bandpass plasmonic filters in a MIM waveguide-resonator system consisting of a MIM bus with arrayed coupled cavities and stub waveguides. The theoretical results show that an obvious electromagnetically induced transparency (EIT)-like transmission spectrum is observable in our plasmonic system, which is in good agreement with finite-difference time-domain (FDTD) simulations. The EIT-like spectral feature is utilized to achieve excellent high-channel-count bandpass filters by the proper architectural design. It is found that the selected wavelengths and bandwidths of our filters can be controlled by adjusting the lengths of stub waveguides and the coupling distances between the cavities and stub waveguides.

## 2. Theoretical modeling

As shown in figure 1(a), the plasmonic configuration consists of a MIM bus and stub waveguides coupling with a rectangular cavity (cavity A). When the incident light is injected into the bus waveguide, the transversal-magnetic (TM) SP mode will be strongly confined in the dielectric layer and propagate along the metal gap. Due to the tunneling effect, the incident light will be coupled into the cavities and excite the resonant modes at special wavelengths. For the waveguide-resonator system, the temporal coupled-mode theory can be utilized to analyze the dynamic transmission characteristics [25, 26]. The amplitudes of the incoming and outgoing waves of the cavity are denoted by $S_{+11}$, $S_{+12}$, $S_{+21}$, $S_{-11}$, $S_{-12}$, and $S_{-21}$, as seen in figure 1(a). When an optical wave with a frequency $\omega$ is launched only from the input port of the bus waveguide ($S_{+12} = 0$), the time-harmonic amplitude $a$ of the cavity can be expressed as

$$\frac{\mathrm{d}a}{\mathrm{d}t} = (-\mathrm{j}\omega_0 - \kappa_0 - \kappa_1 - \kappa_2)a + \mathrm{e}^{\mathrm{j}\theta_1}\sqrt{\kappa_1}S_{+11} + \mathrm{e}^{\mathrm{j}\theta_2}\sqrt{2\kappa_2}S_{+21}, \quad (1)$$

where $\omega_0$ represents the resonance frequency of the Fabry–Perot cavity. $\kappa_0$ are the decay rate due to the internal loss in the cavity, and $\kappa_1$ and $\kappa_2$ are the decay rates due to the energy escape into the bus and stub waveguides, respectively. $\theta_i$ ($i = 1, 2$) is the phase of the coupling coefficient. The dielectric cavity and stub waveguide possess

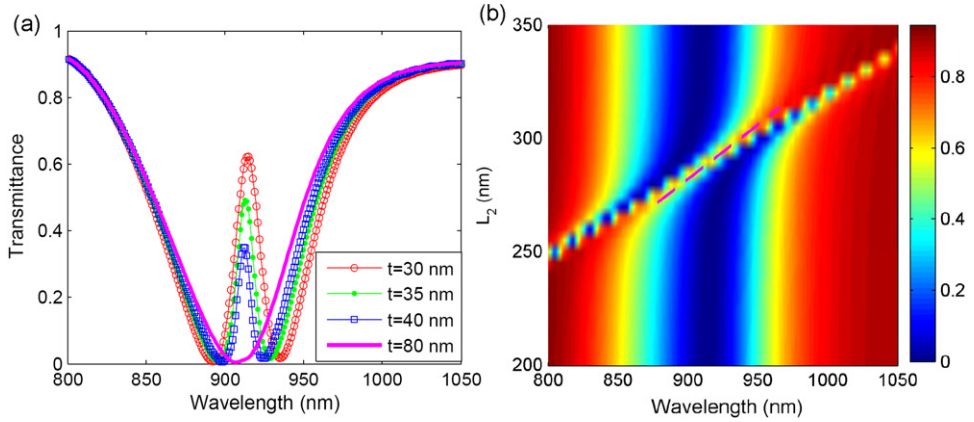


**Figure 2.** (a) Spectral transmittance of the plasmonic waveguide-resonator system with different coupling distance $t$ between the cavity and stub waveguide. The geometrical parameters are $g = 5$ nm, $w = 50$ nm. $L_1 = 250$ nm, and $L_2 = 290$ nm. (b) Evolution of spectral transmittance with the length $L_2$ of stub waveguide when $t = 30$ nm.

mirror symmetry with respect to the reference plane. The incoming and outgoing waves in coupled waveguides should satisfy the following relationships

$$S_{-12} = S_{+11} - \mathrm{e}^{-\mathrm{j}\theta_1}\sqrt{\kappa_1}a, \tag{2a}$$

$$S_{-21} = -S_{+21} + \mathrm{e}^{-\mathrm{j}\theta_2}\sqrt{2\kappa_2}a. \tag{2b}$$

The waves in the stub waveguide should satisfy a steady-state relation: $S_{+21} = \delta \mathrm{e}^{\mathrm{j}\varphi} S_{-21}$. Here, $\delta$ and $\varphi$ are the amplitude attenuation and the phase change between the incoming and outgoing waves of the stub waveguide. Thus, the transmittance efficiency of the waveguide-resonator system can be derived as

$$T(\omega) = \left| \frac{\mathrm{j}(\omega_0 - \omega) + \kappa_0 + \kappa_2(1 - \sigma \mathrm{e}^{\mathrm{j}\varphi})/(1 + \sigma \mathrm{e}^{\mathrm{j}\varphi})}{\mathrm{j}(\omega_0 - \omega) + \kappa_0 + \kappa_1 + \kappa_2(1 - \sigma \mathrm{e}^{\mathrm{j}\varphi})/(1 + \sigma \mathrm{e}^{\mathrm{j}\varphi})} \right|^2. \tag{3}$$

From equation (3), the transmittance is dependent on the phase term $\varphi$ which can be described as: $\varphi = 2L_2\omega\,\mathrm{Re}(n_{\mathrm{eff}})/c + \theta$. Here, $\theta$ stands for the additional phase shift of the stub waveguide, $L_2$ is the length of the stub waveguide and $c$ is the speed of light in a vacuum. $n_{\mathrm{eff}}$ represents the effective refractive index of the fundamental SP mode in the waveguides, which can be obtained by the following dispersion equations [14, 24]

$$\varepsilon_{\mathrm{m}} k_{\mathrm{d}} \tanh\left(\frac{w k_{\mathrm{d}}}{2}\right) + \varepsilon_{\mathrm{d}} k_{\mathrm{m}} = 0, \tag{4a}$$

$$k_{\mathrm{d}} = \sqrt{\beta^2 - \varepsilon_{\mathrm{d}} k_0^2}, \qquad k_{\mathrm{m}} = \sqrt{\beta^2 - \varepsilon_{\mathrm{m}} k_0^2}, \tag{4b}$$

$$n_{\mathrm{eff}} = \beta / k_0. \tag{4c}$$

Here $\varepsilon_{\mathrm{d}}$ and $\varepsilon_{\mathrm{m}}$ stand for the dielectric constant of the insulator and the metal. $k_{\mathrm{d}}$ and $k_{\mathrm{m}}$ are transverse propagation constants in the dielectric and metal, respectively. $w$ is the width of dielectric layers. $\beta$ is the propagation constant of the SP wave. $k_0 = \omega/c$ represents the wavevector of the incident light in vacuum. In our configurations, the metal is assumed as silver, whose frequency-dependent complex permittivity can be described by the well-known Drude model: $\varepsilon_{\mathrm{m}}(\omega) = \varepsilon_\infty - \omega_{\mathrm{p}}^2/[\omega(\mathrm{j}\gamma + \omega)]$. Here $\varepsilon_\infty$ is the dielectric constant at the infinite frequency, $\omega_{\mathrm{p}}$ and $\gamma$ stand for the bulk plasma and electron collision frequencies, respectively. These parameters for silver can be set as $\varepsilon_\infty = 3.7$, $\omega_{\mathrm{p}} = 9.1$ eV, and $\gamma = 0.018$ eV [14]. The insulators in the cavities and waveguides are assumed as air ($\varepsilon_{\mathrm{d}} = 1$). By employing the above theoretical modeling, we investigate the transmission response of the waveguide-resonator system. Figure 1(b) shows spectral transmittance as a function of incident wavelength for different coupling rates between the cavity and stub waveguide. When the decay rate $\kappa_2$ is zero, the effect of the stub waveguide can be neglected. A broad transmitted dip appears at the resonance wavelength of the side-coupled cavity. As the coupling rate increases, it is found that the transmission spectrum possesses a typical EIT-like feature: a narrow transparency peak in the center of a broader transmitted dip [27, 28]. The EIT-like performance is also known as coupled-resonator-induced transparency similar to EIT in the atomic system [29], which is derived from the destructive interference between the two optical pathways passing and bypassing the stub waveguide. The larger coupling rate induces a higher peak transmission and wider spectral bandwidth. From equation (3), it is also important to note that the location of the induced-transparency peak relies on the phase term $\varphi$ of the stub waveguide, which is determined by the length $L_2$. As shown in figure 1(c), the EIT-like peak has a red-shift with the increase of the length of the stub waveguide. The increment of the peak wavelength is almost invariable when the increment of $L_2$ is fixed.

## 3. Numerical experiments and results

The transmission response of the plasmonic configuration is investigated numerically by the FDTD method [30]. The widths of cavity A and waveguides are set as 50 nm. The lengths $L_1$ and $L_2$ are 250 nm and 290 nm, respectively. The coupling distance $g$ between the cavity and bus waveguide is 5 nm. Figure 2(a) shows the spectral transmittance of the configuration with different coupling distance $t$. The smaller

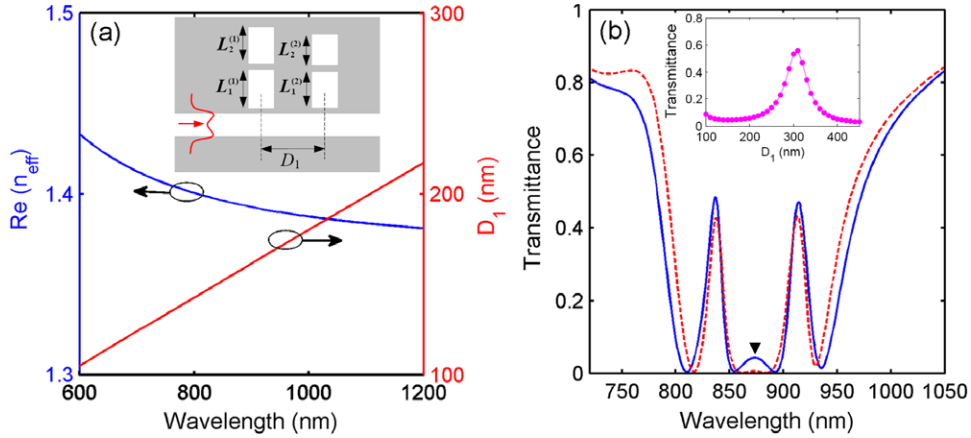


**Figure 3.** (a) Real part of the effective refractive index of the SP mode in the plasmonic waveguide with $w$ of 50 nm. The optimal separation $D_1$ corresponds to the minimal transmittance between the two adjacent transparency peaks. The inset shows the plasmonic configuration with two filtering units. (b) Spectral transmittance of the plasmonic structure with $L_1^{(1)} = 250$ nm, $L_1^{(2)} = 220$ nm (blue and solid), and $L_1^{(1)} = 245$ nm, $L_1^{(2)} = 225$ nm (red and dashed). The other parameters are $L_2^{(1)} = 290$ nm, $L_2^{(2)} = 260$ nm, $D_1 = 155$ nm, $t = 30$ nm, $g = 5$ nm, and $w = 50$ nm. The inset shows the transmittance versus the separation $D_1$.

$t$ corresponds to larger coupling rate between the cavity and stub waveguide. It is found that the spectrum possesses a broad transmitted dip with the coupling distance of 80 nm, which is sufficiently larger than the field skin depth of silver surfaces. The coupling effect of the stub waveguide can be neglected. A narrow transparency peak appears in the transmitted dip and the EIT-like peak becomes wider with the decrease of $t$. The results are in good agreement with the theoretical modeling. Figure 2(b) reveals the evolution of transmission spectrum with the length of stub waveguide. The result shows that a high transmission peak appears in the background of a broad transmitted dip and possesses a nearly linear red-shift, which is consistent with the theoretical results in figure 1(c). The EIT-like transmission response can be utilized to design bandpass plasmonic filters [28], and thus the coupling distance $t$ and the length $L_2$ of the stub waveguide enable control of the filtering features, such as wavelength and bandwidth.

Successively, two filtering units with a separation $D_1$ are integrated into a plasmonic system to investigate the spectral response. As seen in the inset of figure 3(a), the lengths of cavities $L_1^{(1)}$ and $L_1^{(2)}$ are set as 250 nm and 220 nm, and the lengths of stub waveguides $L_2^{(1)}$ and $L_2^{(2)}$ are 290 nm and 260 nm, respectively. The other physical parameters are the same as that in figure 2(a). The two filtering units will generate phase-coupled induced transparency between the adjacent transmitted dips [31]. The phase-coupled induced transparency must be suppressed for excellent wavelength-selective effects. This transparency transmittance is sensitive to $D_1$ and will be quenched due to the destructive interference when the separation $D_1$ equals $\lambda/[4\,\mathrm{Re}(n_{\mathrm{eff}})]$. As depicted in figure 3(a), the real part of $n_{\mathrm{eff}}$ and the optimal $D_1$ are about 1.394 and 155 nm at the wavelength of 874 nm which is marked as '▼' in figure 3(b). The inset of figure 3(b) shows the spectral transmittance as a function of $D_1$ for the incident wavelength of 874 nm. The transmittance is minimal around 155 nm, which verifies the above analysis. We note that the detuning between adjacent transmitted dips influences the spectral transmittance between the two EIT-like peaks. By decreasing the length difference between the adjacent cavities, smaller detuning will lead to the further drop of the transmittance, as shown in figure 3(b). The transmission spectrum exhibits two EIT-like resonance peaks in the broad transmitted dip, which can act as a dual-channel filter. The transmission features are very important for the design of high-count-channel bandpass plasmonic filters.

Figure 4(a) reveals the plasmonic configuration with cascading fundamental filtering units with adjacent separation $D_i$ $(i = 1, 2, \ldots, N-1)$. To exemplify the scalability of the proposed plasmonic filtering structures, four coupled cavities and stub waveguides ($N = 4$) are arrayed to realize four-channel bandpass plasmonic filters. The lengths of cavities are set as 275, 250, 225, and 200 nm. The lengths of stub waveguides are 315 nm, 290 nm, 265 nm, and 240 nm, respectively. The width of waveguides and cavities is 50 nm, the coupling distances between the cavities and stub waveguide are 25 nm, 25 nm, 30 nm, and 35 nm. In order to efficiently depress the transmittance between the EIT-like peaks, the separations between the adjacent cavities are set as 170 nm, 160 nm, and 145 nm. As shown in figure 4(b), the EIT-like spectral peaks exhibit nearly identical interval and height. Meanwhile, the forbidden regions between the peaks are sufficiently low. The transmission characteristics are helpful for a four-channel bandpass plasmonic filter. To further investigate the tunability of the plasmonic filter, we remove the third stub waveguide (i.e. $L_2^{(3)} = 0$ nm) and find that the corresponding pass band around 850 nm is eliminated, as seen in figure 4(c). Figure 4(d) illustrates that the side channels are limited without the first and last stub waveguides, which can be employed to broaden the sidelobes of the plasmonic filters.

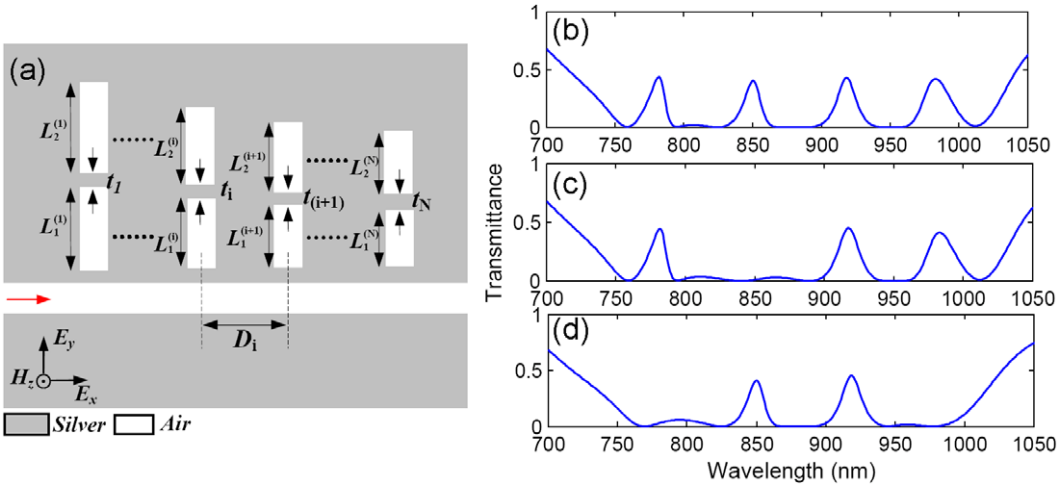


**Figure 4.** (a) Schematic diagram of the plasmonic filtering structure, which consists of arrayed coupled cavities and stub waveguides. (b) Spectral transmittance of the plasmonic waveguide coupled with four cavities and stub waveguides ($N = 4$). The parameters are $g = 5$ nm, $w = 50$ nm, $L_1^{(1)} = 275$ nm, $L_2^{(1)} = 315$ nm, $L_1^{(2)} = 250$ nm, $L_2^{(2)} = 290$ nm, $L_1^{(3)} = 225$ nm, $L_2^{(3)} = 265$ nm, $L_1^{(4)} = 225$ nm, $L_2^{(4)} = 240$ nm, $D_1 = 170$ nm, $D_2 = 160$ nm, $D_3 = 145$ nm, $t_1 = 25$ nm, $t_2 = 25$ nm, $t_3 = 30$ nm, and $t_4 = 35$ nm. (c) Spectral transmittance for $L_2^{(3)} = 0$ nm. (d) Spectral transmittance for $L_2^{(1)} = 0$ nm and $L_2^{(4)} = 0$ nm .

## 4. Conclusions

In this paper, we have proposed a new kind of bandpass plasmonic filter with multiple channels in waveguide-resonator systems. The systems consist of MIM bus and stub waveguides coupled with rectangular cavities. The theoretical modeling shows that the transmission spectral response mimicking EIT can be realized in the plasmonic system with special geometric parameters, as confirmed by FDTD simulations. The EIT-like transmission response enables the realization of ultracompact high-channel-count bandpass plasmonic filters. The filtering wavelengths and bandwidths can be easily controlled by changing the lengths of stub waveguides and the coupling distances between the cavities and stub waveguides, respectively. The proposed configurations may find significant applications in highly-integrated dense wavelength division demultiplexing systems.

## Acknowledgments

This work was supported by the National Natural Science Foundation of China under grants 10874239 and 10604066.

## References

[1] Giannini V, Fernández-Domínguez A, Sonnefraud Y, Roschuk T, Fernández-García R and Maier S 2010 Controlling light localization and light-matter interactions with nanoplasmonics *Small* **6** 2498
[2] Barnes W, Dereux A and Ebbesen T 2003 surface plasmon subwavelength optics *Nature* **424** 824
[3] Bozhevolnyi S, Volkov V, Devaux E, Laluet J and Ebbesen T 2006 Channel plasmon subwavelength waveguide components including interferometers and ring resonators *Nature* **440** 508
[4] Yu Z, Veronis G, Fan S and Brongersma M 2008 Gain-induced switching in metal–dielectric–metal plasmonic waveguides *Appl. Phys. Lett.* **92** 041117
[5] Lu H, Liu X, Wang L, Gong Y and Mao D 2011 Ultrafast all-optical switching in nanoplasmonic waveguide with Kerr nonlinear resonator *Opt. Express* **19** 2910
[6] Veronis G and Fan S 2005 Bends and splitters in metal–dielectric-metal subwavelength plasmonic waveguides *Appl. Phys. Lett.* **87** 131102
[7] Wang B and Wang G 2004 Surface plasmon polariton propagation in nanoscale metal gap waveguides *Opt. Lett.* **29** 1992
[8] Nikolajsen T, Leosson K and Bozhevolnyi S 2004 Surface Plasmon polariton based modulators and switches operating at telecom wavelengths *Appl. Phys. Lett.* **85** 5833
[9] Enoch S, Quidant R and Badenes G 2004 Optical sensing based on plasmon coupling in nanoparticle arrays *Opt. Express* **12** 3422
[10] Randhawa S, González M, Renger J, Enoch S and Quidant R 2010 Design and properties of dielectric surface plasmon Bragg mirrors *Opt. Express* **18** 14496
[11] Leon I and Berini P 2010 Amplification of long-range surface plasmons by a dipolar gain medium *Nature Photon.* **4** 382
[12] Gan Q, Ding Y and Bartoli F 2009 'Rainbow' trapping and releasing at telecommunication wavelengths *Phys. Rev. Lett.* **102** 056801
[13] Park J, Kim H and Lee B 2008 High order plasmonic Bragg reflection in the metal–insulator–metal waveguide Bragg grating *Opt. Express* **16** 413
[14] Han Z, Forsberg E and He S 2007 Surface plasmon Bragg gratings formed in metal–insulator–metal waveguides *IEEE Photon. Technol. Lett.* **19** 91
[15] Neutens P, Dorpe P, Vlaminck I, Lagae L and Borghs G 2009 Electrical detection of confined gap plasmons in metal–insulator–metal waveguides *Nature Photon.* **3** 283
[16] Zia R, Schuller J, Chandran A and Brongersma M 2006 Plasmonics: the next chip-scale technology *Mater. Today* **9** 20
[17] Lin X and Huang X 2008 Tooth-shaped plasmonic waveguide filters with nanometeric sizes *Opt. Lett.* **33** 2874
[18] Lu H, Liu X, Mao D, Wang L and Gong Y 2010 Tunable bandpass plasmonic waveguide filters with nanodisk resonators *Opt. Express* **18** 17922

[19] Hosseini A and Massoud Y 2007 Nanoscale surface plasmon based resonator using rectangular geometry *Appl. Phys. Lett.* **90** 181102
[20] Wang T, Wen X, Yin C and Wang H 2009 The transmission characteristics of surface plasmon polaritons in ring resonator *Opt. Express* **17** 24096
[21] Noual A, Akjouj A, Pennec Y, Gillet J and Djafari-Rouhani B 2009 Modeling of two-dimensional nanoscale Y-bent plasmonic waveguides with cavities for demultiplexing of the telecommunication wavelengths *New J. Phys.* **11** 103020
[22] Lu H, Liu X M, Gong Y K, Mao D and Wang L R 2011 Enhancement of transmission efficiency of nanoplasmonic wavelength demultiplexer based on channel drop filters and reflection nanocavities *Opt. Express* **19** 12885
[23] Zhou L, Yu X and Zhu Y 2006 Propagation and dual-localization of surface plasmon polaritons in a quasiperiodic metal heterowaveguide *Appl. Phys. Lett.* **89** 051901
[24] Gong Y, Liu X and Wang L 2010 High-channel-count plasmonic filter with the metal–insulator–metal Fibonacci-sequence gratings *Opt. Lett.* **35** 285
[25] Haus H 1984 *Waves and Fields in Optoelectronics* (Englewood Cliffs, NJ: Prentice-Hall)
[26] Piao X, Yu S, Koo S, Lee K and Park N 2011 Fano-type spectral asymmetry and its control for plasmonic metal–insulator–metal stub structures *Opt. Express* **19** 10907
[27] Lu H, Liu X, Mao D, Gong Y and Wang G 2011 Induced transparency in nanoscale plasmonic resonator systems *Opt. Lett.* **36** 3233
[28] Xu Q, Sandhu S, Povinelli M, Shakya J, Fan S and Lipson M 2006 Experimental realization of an on-chip all-optical analogue to electromagnetically induced transparency *Phys. Rev. Lett.* **96** 123901
[29] Totsuka K, Kobayashi N and Tomita M 2007 Slow light in coupled-resonator-induced transparency *Phys. Rev. Lett.* **98** 213904
[30] Taflove A and Hagness S C 2000 *Computational Electrodynamics: the Finite-Difference Time-Domain Method* (Boston, MA: Artech House Publishers)
[31] Kekatpure R, Barnard E, Cai W and Brongersma M 2010 Phase-coupled plasmon-induced transparency *Phys. Rev. Lett.* **104** 243902